Particle Detectors at the LHC

Before we begin our discussion of QCD at the LHC, there is one more issue that we need to discuss. Now that we have discussed the general properties of events at a 14 TeV pp collider, we need to understand what about these events is actually measurable. In this lecture, I will present an overview of the two high-energy collider detectors at the LHC – ATLAS and CMS – and review their projected capabilities.

Figs p. 2 shows the general plan of the LHC. The accelerator contains two rings of magnets (actually, a single ring with two magnetic apertures), circulating protons in opposite directions. The ring circumference is 27 km, the bending field is 7 T. This allows an energy per particle of 7 TeV. The two beams cross at a maximum of 8 points around the ring. Two of these points house the huge, general purpose detectors ATLAS and CMS. Two more intersection points house special-purpose experiments — LHC-b, for rare B and Λ_b decays, and ALICE, for studies of heavy-ion collisions. In this course, we will concentrate on high transverse momentum processes, for which the ATLAS and CMS detectors are most relevant.

There are some excellent references that describe the capabilities of these two experiments, to the extent that these can be understood in advance of the data-taking. Both ATLAS and CMS have issued Physics and Detector Performance Technical Design Reports (TDR's). Recently, both experiments issued formal review articles documenting their detectors, published in the journal JINST. Links to these references are provided on the course Web site. In my discussion here, I will emphasize ATLAS, giving a comparison to CMS where it is relevant. (The question of which detector is "better" is subtle and multifaceted — and should wait for the actual data analysis.)

Before beginning a discussion of the detectors, we should examine the expected event rates and their time structure. The design luminosity of the LHC is

$$\mathcal{L} = 10^{34} / \text{cm}^2 \text{sec}$$

Multiply by the length of a year that includes inefficiencies and shutdowns, conventionally 10^7 sec, this gives

$$\int dt\, \mathcal{L} = 10^{41}\ \text{cm}^{-2} = 100\ \text{fb}^{-1}$$

that is, 100 events/yr for a process whose cross section is 1 fb. The first few years of LHC running are planned to be at a lower luminosity $\mathcal{L} = 10^{33} / \text{cm}^2 \text{sec}$, corresponding to

$10\ fb^{-1}$/year.

The protons in the LHC are accelerated in bunches, spaced 25 nsec apart. (1 nsec ~ 1 foot). Every 25 nsec, then, a bunch reaches the interaction point and hits a bunch from the other beam. This is a bunch crossing rate of 40 MHz (4×10^7 /sec.). The integrated luminosity per bunch crossing is then

$$\Delta \int \mathcal{L} = 2.5 \times 10^{26}\ cm^{-2} = 0.25\ mb^{-1}$$

This sounds like not very much, until you realize that $\sigma_{tot}(pp) = 100 mb$, giving 25 pp collisions (20 inelastic) per bunch crossing! The beams cross in a luminous region of length 8 cm

so it is possible to separate these collisions, but it is difficult. At the nominal low luminosity, we still have ~ 2 inelastic pp events in every bunch crossing.

The torrent of events is a scary feature of LHC physics. In ATLAS, when a bunch collision is taking place, the products of the previous collision are still in active regions of the detector (8m away), and muons from the collision before that are still passing through the outer detector. Every element

of the detector must respond quickly if we are not to be very confused.

Figs. pp. 3,4 show the general plans of the ATLAS and CMS detectors. They are huge! ATLAS is 10 stories high. CMS (the "compact muon solenoid") is more compact — it is 5 stories high. Both detectors follow the general plan for collider detectors first introduced in the Mark I detector at the SPEAR storage ring at SLAC. Various particle identification devices are constructed in concentric cylinders to perform different measurements on the final particles. The general idea is shown in Fig. p. 5 (I thank John Conway for this figure.) The central region contains a low-density material that can be ionized by charged particles and a solenoidal B field that bends these particles. By visualizing the tracks and measuring the bends, we determine the particle momenta. The next layer contains a highly segmented high-Z material to convert gamma rays and electrons into observable ionization. This "EM calorimeter" measures the energies of electromagnetic components of the event. (At a hadron collider, these are mainly γ rays from $\pi^0 \to 2\gamma$ decays.) Outside of this, there is a thicker region of material to convert the energies of hadrons to ionization ("hadron calorimeter"). The hadron calorimeter

should be sufficiently thick that only highly penetrating muons can get through it. On the very outside of the detector, there might be special-purpose devices that track these muons.

Figs. 6,7 show how these devices are laid out in ATLAS and CMS. In ATLAS (Figs p.6), there is a central cylinder of tracking devices in a 2T solenoidal magnetic field. Outside the magnetic, there is a Pb-liquid Ar electromagnetic calorimeter, followed by an Fe-scintillating tile hadron calorimeter. Finally, on the outside of the detector, there is a set of magnets that set up a toroidal magnetic field. A muon that reaches this region is bent in a plane orthogonal to its bending in the interior of the detector, providing a complementary measurement of its momentum.

In CMS (Fig. p.7) the EM and hadron calorimeters are placed inside magnet, and a higher field (4T.) is used. The EM calorimeter is a set of $PbWO_4$ crystals that promise very high resolution. The hadron calorimeter is a Cu-scintillator device that is required to be rather thin to fit inside the magnet coil. The outer part of the detector is an iron absorber with chambers to measure muons and deeply penetrating hadrons. The iron returns the magnetic flux from the solenoid, so it contains a weaker field than in the center, in the opposite direction. A muon thus bends in one direction in the

central region and oppositely in the outer region, again providing complementary momentum measurements.

Let me now go into more detail on each of these devices. First consider the interior tracking volume. For a particle of unit charge, the Lorentz force equation gives, for very relativistic motion,

$$\frac{dp_T}{dl} = (300 \frac{MeV}{T\text{-}m}) \cdot B \cdot E$$

This gives a radius of curvature $R(m) = 3.3\ E(GeV)/B(T)$

However, for very energetic particles, a detector sees only a small part of the circle. A better formula, is

$$\frac{s}{R} = \frac{1}{2}\left(\frac{l}{2\pi R}\right)^2 .$$

or

$$s = (3.8\ mm) \cdot \frac{B(T)\, l^2(m)}{E(GeV)}$$

s is called the "sagitta" of the track. To obtain the best momentum measurement, it is necessary to make Bl^2 as large as possible, and then to have a high-precision device to measure the track positions. This device should also be as thin as possible to avoid scattering the particles and disrupting the trajectory.

ATLAS and CMS both do the tracking with silicon elements that give a point resolution of 10-20 μ. In ATLAS, there are three nested devices.

Pixel (2D) sensors — 3 layers at 4 cm, 10 cm, 13 cm

Silicon strips — 4 layers at 15 - 56 cm

Straw tubes 64 - 103 cm.

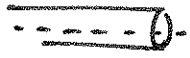

The last of these is a more conventional ionization technology. However, it measures "transition radiation" which depends on the γ of the particle and so provides e/π discrimination. Figs. p.8 gives a picture of the ATLAS tracking system. Figs. p.9 show the layout in (r, θ) and (r, η). Notice that the central detector goes only to $\eta = 1.5$, but that there are forward detectors, oriented in rings around the beam axis, that cover the region up to $\eta = 2.5$. Figs. p. 10 shows the design of the toroidal muon spectrometer, covering a region from 5 to 10 m from the beam axis. There are also forward discs that track muons up to $\eta \sim 2.5$.

The projected accuracy of the muon momentum measurement in the inner detector (from the TDR) is

$$\sigma\left(\frac{1}{p_T}\right) = \frac{\sigma(p_T)}{p_T^2} = 3.6\times10^{-4} \oplus \frac{1.3\times10^{-2}}{\sqrt{p_T^2 \sin\theta}} \quad (GeV^{-1})$$

This gives

$$\frac{\sigma(p_T)}{p_T} = \begin{cases} 0.4\,\% & \text{for a } 10\ GeV/c\ \mu \\ 3.6\,\% & \text{for a } 100\ GeV/c\ \mu \end{cases}$$

The outer muon system gives a longer moment arm to measure the sagitta for a very high momentum muon. Using this system also, we have

$$\frac{\sigma(p_T)}{p_T} = \begin{cases} 2\,\% & \text{for a } 100\ GeV/c\ \mu \\ 10\,\% & \text{for a } 1\ TeV/c\ \mu \end{cases}$$

Figs. p. 11 shows the expectation for the width of the Z in $Z \to \mu^+\mu^-$. This is only a small degradation of the intrinsic Z width. Figs. p. 12 shows the expected probability of incorrect sign determination for very high energy muons, reading a track with curvature γ as one with the opposite curvature.

The next device as we go outward is the EM calorimeter. To understand the parameters of the devices, let's first discuss the physics of EM calorimetry. A γ or $e^\pm$ with energy above 1 MeV, as it goes through matter, will radiate or convert in the field of a heavy nucleus:

$$\gamma \to e^+e^- \qquad e^- \to \gamma e^-$$

The characteristic distance for these processes is called the radiation length X_0. X_0 depends on the nucleus

charge of the material as $X_0 \sim Z^{-2}$, so it is good to have high Z and dense materials. In a few X_0, the initial e^+ or γ becomes a shower with many e^+, e^-, γ; this shower must have a depth of $10X_0$ or more. Measurement of the total ionization produced in a shower gives the energy of the initial particle.

In ATLAS, the EM calorimeter is built from pieces of Pb, for which $X_0 = 0.56$ cm, immersed in liquid Ar, an inert liquid that can pick up and transport ionization. A plan of the calorimeter is shown in Figs. p. 13. The central barrel covers r from 1.3 m to 2.3 m, giving a depth of $24X_0$. A forward calorimeter covers the region up to $\eta \sim 4$. Note the gap at $\eta \sim 1.5$, where the two pieces 'join'. Electronics, cryogenic pipes, and other necessary services, run through this gap. This is a weak point in the calorimetry, but the reality of detector construction makes such weak points necessary.

Lead (Pb) is an excellent material for an EM calorimeter because of its short X_0, but it is also an absorber of the ionization in the shower. The liquid Ar gaps between the Pb elements allow us to sample the ionization of the shower. The statistics of this sampling typically dominates the calorimeter resolution; thus, $\sigma \sim \sqrt{E}$. For the ATLAS EM calorimeter, test beam data such as that in Fig. p. 14 can be summarized by the

formula (Figs. p. 15)

$$\frac{\sigma}{E} = \frac{10.1\%}{\sqrt{E}} \oplus 0.17\% \qquad E \text{ in GeV}$$

The calorimeter (and the hadron calorimeter behind it) are highly segmented in (η,ϕ), with $\Delta(\eta,\phi) \sim 0.01$. This is about 10 times finer (η,ϕ) resolution than that of the Tevatron detectors.

CMS chose a different strategy for EM calorimetry. Instead of a sampling device, they have an array of crystals of $PbWO_4$. These are transparent crystals with very short X_0. The nominal performance is shown in Figs. p. 16

$$\frac{\sigma}{E} = \frac{3.6\%}{\sqrt{E}} \oplus \frac{124\,\text{MeV}}{E} \oplus 0.26\% \qquad E \text{ in GeV}$$

This is well superior to ATLAS. There are some compensating disadvantages; because the crystals are not segmented in depth, they are poorer at measuring the first stages of a hadronic shower as a contribution to the hadron calorimetry.

One task of the EM calorimeter is to pick out direct photons, as opposed to photons resulting from $\pi^0 \to 2\gamma$ decay. This is especially important for the Higgs boson search in $h^0 \to 2\gamma$. A π^0 is seen as two γ's that typically create overlapping showers. Thus, the shape of the energy deposition in the EM calorimeter gives some π^0/γ discrimination. The expected π^0 rejection

is a factor 3-4, as shown in the left-hand panel of Figs. p. 17 (from the TDR). A much more powerful source of discrimination is the fact that π^0's are usually found in jets. Applying the criterion that a direct photon should be isolated from other produced particles, we obtain the factor of 3000. rejection shown in the right-hand panel.

Behind the EM calorimeter is a larger device with lower Z and coarser segmentation, the hadron calorimeter. The full calorimeter plan in ATLAS is shown in Figs. p. 18. The hadron calorimeter is also a sampling calorimeter, with Fe as the main material and scintillating tiles as the detectors. The performance for $\pi^\pm$ is shown in Figs. p. 19

$$\frac{\sigma}{E} = \frac{56\%}{\sqrt{E}} \oplus 5.5\% \qquad E \text{ in GeV}$$

Hadron calorimetry is very subtle. The basic idea is that, if hadrons scatter from nuclei, eventually their energy is converted into π^0's which rapidly decay, leady to electromagnetic cascades. However, there is a mismatch of scales. In Fe,

$X_0 = 1.76$ cm, but the nuclear interaction length

$\lambda_I = 16.8$ cm. It is difficult to have enough Fe to contain the shower while having thin enough pieces to obtain good sampling of the electromagnetic component. In addition,

hadronic collisions can break up nuclei, absorbing energy that does not appear in an electromagnetic cascade. The response of a calorimeter to an incident π^+ will be different if the π^+ converts to a π^0 in its first collision or converts to a π^0 only after several collisions. Fig. p.20 shows a quantity that measures this effect, the ratio of the calorimeter response to an incident e^- or an incident π^+. There are strategies to correct for this differential response either by using a different material in the calorimeter (DØ uses Uranium, which is neutral with respect to nuclear breakup) or by observing the history of the hadronic shower and using this information to make a correction.

Actually, what we really want is not the energy of an individual hadron but the energy of a jet initiated by a quark or gluon. This brings in more complications. Jets may fluctuate from having a leading π^+ to having a leading π^0. Jets also contain particles such as n or K_L that may not interact until deep in the hadron calorimeter. The projected ATLAS energy resolution for jets (from the TDR) is:

$$\frac{\sigma}{E} = \frac{81\%}{\sqrt{E}} \oplus 1.7\% \oplus \frac{3.9}{E} \qquad (E \text{ in GeV})$$

Additional complications come from QCD. There are subtleties in defining what hadrons should or should not be included in a jet.

These are dealt with in the above formula using a fixed convention. I will discuss these issues in some detail later in the course.

Since the various elements of the detector lie one inside the other, the presence of elements inside can affect, and will usually degrade, the performance of the detectors outside. Material in the tracking system will cause γ's to convert in front of the EM calorimeter. Material in the EM calorimeter will initiate hadronic showers that then extend into the hadron calorimeter. Figs p. 21, 22, 23 present three views of this issue for the ATLAS detector. Figs p. 21 show the material in the inner detector, in X_0 and in λ_I, as a function of η. In the barrel region of the detector, the impact is modest, $X_0 \sim 0.5$ and $\lambda_I \sim 0.2$, but in the forward region there can be substantial material in front of any active element. The peak at $\eta \sim 1.5$ represents the cryostats of the silicon devices. Figs. p. 22 show the material in front of and then within the EM calorimeter, in units of X_0. The magnet coil (which is inside the EM calorimeter in ATLAS but outside in CMS) contributes almost 2 units of X_0. Finally, Figs. p. 23 show the thickness of the detector as a function of η in units of λ_I. It is interesting that the forward calorimeters are very thick and also highly segmented, giving

good purely calorimetric measurements out to $\eta \sim 4.5$.

To complete our understanding of the LHC detectors, we should discuss three more specialized issues — missing energy, tagging of b and τ, and triggering.

Many models of new physics, especially those that address the problem of dark matter, predict the production of invisible particles. Events with invisible, weakly interacting particles, will in general show unbalanced momentum. Thus it is interesting to understand to what extent the detectors can be sensitive to momentum imbalance. I have already discussed the fact that hadron-hadron collisions produce many particles in the beam direction that are emitted at angles too small to be detected. So it is hopeless to measure longitudinal momentum balance. We must concentrate on measuring missing transverse momentum, often denoted $\not{E}_T$ or MET.

Figs. p. 24 shows the projected $\not{E}_T$ resolution in ATLAS. This is of the same order as the calorimeter resolution

$$\frac{\sigma}{(\sum E_T)} = \frac{53\%}{\sqrt{\sum E_T}}$$

However, we are most concerned with rare events with large $\not{E}_T$ and whether these can be generated by fluctuation or

mismeasurements of Standard Model events. To avoid large spurious $\not{E}_T$, we must first of all have a working, well-understood detector. Noise can be a source of $\not{E}_T$; this must be understood and controlled. A problem at the next level is illustrated in Figs. p. 25, from the ATLAS TDR. This figure shows a simulation of

$$pp \to Z^0_{\hookrightarrow \mu^+\mu^-} + \text{jet}.$$

In general, the momentum balance between the Z^0 and the jet is expected to be good, but there are rare events where the imbalance can be 150 – 200 GeV. The right-hand plot shows the η of the jet in cases with large $\not{E}_T$ imbalance. Often, the jet points to the join region at $\eta \sim 1$ where the calorimetry is poorest. Eventually, we can learn to identify cases where $\not{E}_T$ is likely to come from mismeasurement rather than new physics. Figs p.26 shows an example of this in a DØ supersymmetry search. The data show an excess above the Standard Model for dijet events with large $\not{E}_T$. However, the excess is seen only in the region where the two jets are back to back in ϕ, an indication that the $\not{E}_T$ is coming from mismeasurement of one jet in a simple QCD two-jet event.

Next, discuss b and τ identification. The b quark has a long lifetime on strong interaction time scales:

$$\tau = 1.5 \text{ psec} \quad \text{or} \quad c\tau = 0.46 \text{ mm}$$

Typical b quarks in jets will have a path length $\gamma c\tau$ of many mm. Using precision tracking — in particular, the very precise pixel detector — we should be able to identify tracks from b decay as coming from vertices displaced from the beam crossing region. Various ways to make this identification are shown in Figs. p.27. We might be able to show that pairs or triplets of tracks intersect in a secondary vertex. Alternatively, we can measure the impact parameter of tracks relative to the primary vertex and show that there is a displacement larger than could be accounted for by measurement error. The vertex is displaced by $\gamma c\tau$ as the b's have higher energy, but the method requires find several high-quality tracks. The impact parameter is always of the order of $c\tau$ but it can be measured for each track.

Figs. p.28 shows the lego plot for a 2-jet event at CDF. Figs. p.29 shows a close-up view of the track-finding for this event. (The inner layer of silicon wafers is at 1cm from the beam spot.) You can see that the high momentum tracks shown emated from two displaced vertices, so this is likely to be a $p\bar{p} \to b\bar{b} + X$ event.

Very often, the distribution of vertices or impact parameters is plotted in terms of the variable

(impact parameter)/σ or LIP/σ

where σ is the error expected from the tracker. If the track is in a jet, the impact parameter can be given a sign

positive: 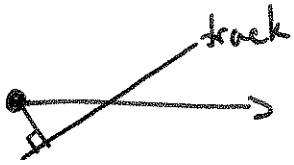

negative: 

depending on whether the apparent vertex would be ahead of behind the beam spot. Negative impact parameters are generated only by tracking errors, so the distribution of negative impact parameters should measure σ and should be the same for b quark jets and light quark jets. Figs. p. 30 show the distribution of a variable that is essentially (IP/σ) for tracks in $e^+e^- \to q\bar{q}$ at the Z^0 resonance. The histograms indicate a separation of the measured distribution into a symmetric component from $q = u, d, s$, a component with a short but nonzero lifetime from c, and a component with a long lifetime from b. Figs. p. 31 shows the comparable distributions measured by DØ for QCD jets and for b-quark jets at the Tevatron. Figs p. 32 shows the expectation for ATLAS.

If we cut harder on IP/σ we obtain a cleaner sample of b-quark jets, but we lose statistics. So the b-quark tagging efficiency is not a fixed number but rather is given by an efficiency/purity tuning curve. The optimal position on the curve depends on the analysis (What is the signal cross section? What backgrounds must

be overcome?) Figs p. 33 show efficiency vs. purity curves from the ATLAS TDR. Since we are usually trying to find b jets in a much larger sample of light quark and gluon jets, it is difficult to achieve a b-tagging efficiency higher than about 30-40%.

The τ has a shorter lifetime; $c\tau = 0.09$ mm, too short for this to be a reliable means of identification. Instead, we look at special properties of the τ final states. The τ decay modes

$$\tau \to e \bar{\nu}_e \nu_\tau \qquad \tau \to \mu \bar{\nu}_\mu \nu_\tau$$

are difficult to distinguish from direct e, μ production. But the τ also can decay to low mass hadrons

$\tau^- \to \pi^- \nu$	BR = 11.6%	
$\tau^- \to \rho^- \nu$	BR = 22.5%	$\rho^- \to \pi^- \pi^0$
$\tau^- \to a_1^- \nu$	BR = 18%	$a_1^- \to \pi^- \pi^0 \pi^0$, $\pi^- \pi^- \pi^+$

The tau is a lepton, so it is produced isolated from particles that might form a hadronic jet. This suggests the identification strategy shown in Figs p.34: Look for a very narrow jet containing only 1(or 3) energetic charged particles. Insist that the charged particles are close to the calorimetrically-determined jet axis. Insist that, in a larger angular region around the narrow core, very little energy is deposited. Then the jet is likely to be a τ. Figs p.35 show the selection efficiency vs. the isolation

cone size in (η, ϕ).

In hadronic τ decays, the hadrons carry off most of the energy of the tau. The energy transfer is not perfect, of course, but the distribution is known and is heavily peaked toward $E_{had}/E_\tau = 1$. This distribution can be used to reconstruct heavy particles that decay to τ. See Figs. p. 36.

Finally, we need to discuss the trigger. I have noted already that the LHC detectors receive events at the rate of 40 MHz. Only a small fraction of these events can be written to permanent storage. The event data size is about 1.5 Mb, so a 200 Hz data storage rate already yields

$$1.5\ \text{Mb} \times 200/\text{sec} \times 10^7\ \text{sec/yr} = 3\ \text{Pb/yr}$$

which is a formidable amount of data. (The BaBar data set is a few hundred Tb.) To achieve this we need an automatic way to choose which 200 events out of 40 million we save each second. The remaining events are simply thrown away, so if the experiments do not choose correctly they might as well not have taken the data.

When the events are recorded, they are put temporarily into a data pipeline. Then a series of computers analyzes properties of the events and generates decisions to discard the events or pass them on to the next stage. In ATLAS, the trigger has 3 stages, each of which must achieve about a factor 100 in

reduction of the number of events:

		decision time:
Level 1:	looks for large calorimetric p_T deposits or high p_T muons	100 μsec / event
Level 2:	tries to assemble jets, looks for missing E_T, b-tags isolated μ e τ	10 msec / event
Level 3:	full event reconstruction	1 sec / event

So each level applies increasingly sophisticated criteria to obtain good-quality and interesting events. In principle, any process with cross section less than 100 nb (eg. $Z \to l^+l^-$, $t\bar{t}$ production) should be accepted by the trigger with little inefficiency. The menu of trigger criteria also includes "prescaled" triggers, in which more common processes are accepted with lower probability. These are used to understand the more common classes of events, and to check that the trigger is working correctly. For example, the trigger might accept 1 "minimum bias" event each second.

Fig. p. 37 shows a more detailed plan of the ATLAS trigger system.